

Late superhumps and the stream-disc impact in IY UMa

Daniel J. Rolfe,¹ Carole A. Haswell,¹ and Joseph Patterson²

¹*Department of Physics and Astronomy, The Open University, Walton Hall, Milton Keynes MK7 6AA*

²*Department of Astronomy, Columbia University, 538 W. 120th St., New York, New York 10027*

Submitted July 2000

ABSTRACT

We use the hot spot eclipse times of the newly discovered deeply-eclipsing dwarf nova IY UMa to trace out the shape of its disc during the late superhump era. We find an eccentric disc. We show that the brightness of the stream-disc impact region varies as expected with $|\Delta\vec{V}|^2$, where $\Delta\vec{V}$ is the relative velocity of the stream with respect to the velocity of the disc at the impact point. We conclude that the hot spot is the source of late superhump light.

Key words: accretion discs – binaries: close – binaries: eclipsing – stars: individual: IY UMa – stars: cataclysmic variables

1 INTRODUCTION

IY UMa was identified as a dwarf nova type cataclysmic variable (CV) in January 2000 (Uemura et al. 2000) when it went into superoutburst showing strong superhumps and deep eclipses in its lightcurve.

Superhumps are luminosity variations with period, P_{sh} , a few percent longer than the orbital period, thought to arise from the interaction of the donor star orbit with a slowly progradely precessing non-axisymmetric accretion disc. The eccentricity of the disc arises because a 3:1 resonance occurs between the donor star orbit and motion of matter in the outer disc. This can only occur in systems with a sufficiently low mass ratio ($q = \frac{M_{\text{donor}}}{M_{\text{wd}}}$) that the 3:1 resonance radius is within the tidal radius at which the disc is truncated by tidal forces (Paczynski 1977). The superhump period is then given by

$$\frac{1}{P_{\text{sh}}} = \frac{1}{P_{\text{orb}}} - \frac{1}{P_{\text{prec}}}$$

where P_{prec} is the disc precession period and P_{orb} is the orbital period.

A detailed study of the superoutburst of IY UMa was carried out by Patterson et al. (2000) (hereafter P2000). IY UMa has orbital period $P_{\text{orb}} = 1.77$ hours. The system parameters were estimated in P2000 as $M_{\text{wd}} = 0.86 \pm 0.11 M_{\odot}$, $M_{\text{donor}} = 0.12 \pm 0.02 M_{\odot}$ and orbital inclination $i = 86^{\circ}8 \pm 1^{\circ}5$.

2 OBSERVATIONS

Here we analyse V-light data covering the late superhump era, HJD 2451572–79, from the more extensive data presented in P2000. These data comprise 22 eclipses with typi-

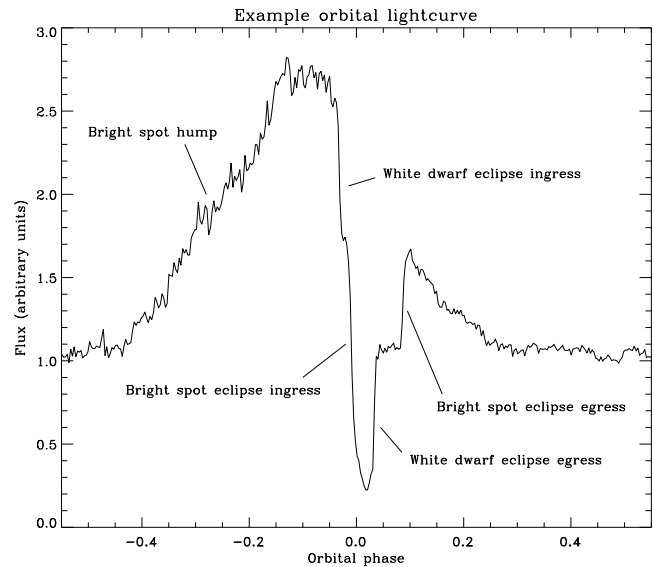


Figure 1. An example orbital lightcurve of IY UMa during the late superhump era which clearly shows the white dwarf and hot spot eclipse ingresses and egresses. This orbit has mid-eclipse at HJD 2451578.69.

cal time resolution 20 to 30 seconds. Figure 1 shows a representative orbital lightcurve, where a strong orbital hump is visible as the stream disc impact region (bright spot) comes into view before eclipse. The white dwarf and hot spot eclipses are easily identified.

The entire dataset being analysed is shown in Figure 9a, and is discussed in Section 5.

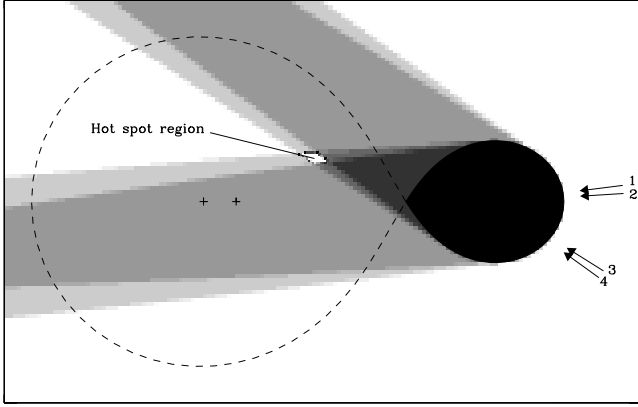


Figure 2. “Shadows” cast by the donor star at the beginning and end of hot spot ingress (observer looking from 1 and 2 respectively) and at start and end of hot spot egress (3 and 4) constrain the location of the hot spot in the orbital plane to a diamond shape.

3 TRACING THE ECCENTRIC DISC SHAPE

3.1 Shadow method

The eclipse of the prominent hot spot (Figure 1) provides an opportunity to probe the disc shape. Assuming the surface of the donor star is described by its Roche potential surface, and if the mass ratio, q , and orbital inclination, i , are known, the region of the orbital plane eclipsed by the donor at any particular orbital phase can be calculated. Figure 2 shows how these “shadows” cast by the donor star at phases corresponding to the start and end of hot spot eclipse ingress and egress constrain the location of the hot spot in the orbital plane to a diamond shaped region. This method has been used before, e.g. Wood et al. (1986). The hot spot is the point where the accretion stream impacts the edge of the disc, so determining the hot spot location determines the location of the disc edge. Assuming the disc precesses at the beat period between the orbital and superhump periods, the geometry shown in Figure 4 was used to trace out the outline of the disc edge using those eclipses where both ingress and egress of hot spot eclipse could be measured.

3.2 Stream trajectory method

For some eclipses, only the egress of hot spot eclipse could be measured, and so the technique described above could not be employed for those eclipses. However there is an alternative technique for determining the location of the hot spot which can be employed in this situation (Hessman et al. 1992). Since the hot spot lies on the accretion stream, and the times of hot spot egress depend on the distance of the hot spot from the line of centres of the two stars, a ballistic trajectory for the accretion stream can be used to infer the position of the hot spot along the stream. Hence the location of the hot spot and the disc edge can be determined. Figure 3 shows the variation of eclipse egress phase along a ballistic stream trajectory.

The uncertainty in the time of each point of contact translates mostly to an error in the radial distance of the hot spot from the white dwarf for an assumed q . Azimuthal error was estimated by considering three slightly different stream

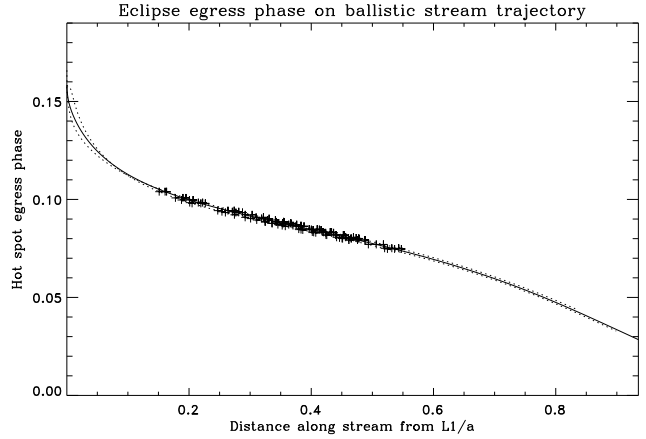


Figure 3. Orbital phase of eclipse egress for points on a ballistic stream trajectory calculated assuming the shape of the donor star to be described by its Roche potential surface. The solid curves represent a stream started from the L1 point with $(V_x, V_y) = (-C_s, 0)$ (see Section 3.2) while the dotted curves are streams started with $(V_x, V_y) = (-C_s, \pm C_s)$. The crosses are the measured egress phases at their inferred positions along the stream.

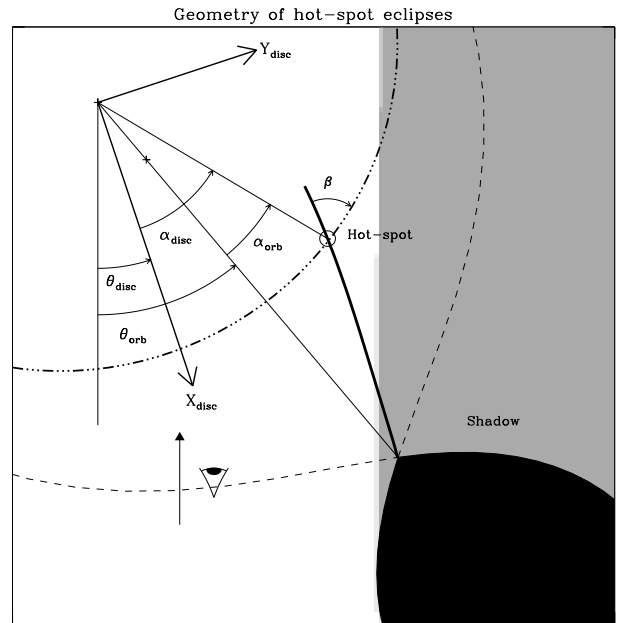


Figure 4. The geometry of the system used to study the hot spot eclipses. This figure shows the situation at orbital phase 0.11, shortly after a hot spot eclipse. The disc coordinates (X_{disc}, Y_{disc}) are centred on the white dwarf. The stream impacts the disc edge (thick dot-dashed outline) at the hot spot, at angle α_{orb} to the line of centres of the two stars, which itself makes an angle θ_{orb} with the line of sight. The X-axis of the disc makes an angle θ_{disc} with the line of sight, and so the position of the stream-disc impact in the precessing disc frame makes an angle $\alpha_{disc} = \alpha_{orb} + \theta_{orb} - \theta_{disc}$ with the disc X-axis. β is approximately the angle between the stream and disc velocities at the point of impact.

trajectories with initial velocities at the inner Lagrange point (with axes as shown in Figure 5) of $(V_x, V_y) = (-C_s, 0)$, $(-C_s, C_s)$ and $(-C_s, -C_s)$. C_s is the sound speed at the L1 point estimated using

$$C_s \approx 10^4 \text{ m s}^{-1} \sqrt{\frac{T}{10^4 \text{ K}}}$$

where the photospheric temperature T comes from the stellar models by Baraffe (Baraffe et al. 1998). The different hot spot positions coming from these three slightly different trajectories provide the small near-azimuthal error bars on the egress and ingress locations in Figure 5.

3.3 Combining the methods

The disc radius determined using the stream trajectory method depends on whether the start, middle or end of egress is used. We find that for those eclipses where both ingress and egress were measured, using the mid-egress times to locate the hot spot on the accretion stream gives results consistent with the robust ‘‘shadow’’ method whose results completely constrain the location of the hot spot in the orbital plane. We therefore use the shadow method to determine hot spot location and disc radius for those eclipses where both hot spot ingress and egress are measurable, and the stream trajectory method with mid-egress time for the remaining eclipses.

We use the white dwarf mid-eclipse ephemeris $T_{mid} = HJD\ 2451570.85376(2) + 0.07390906(7)E$ and late superhump maximum ephemeris $T_{mid} = HJD\ 2451571.731(3) + 0.07558(6)E$ from P2000 to calculate orbital phase and superhump phase. The beat phase between orbital and superhump phase, interpreted as disc precession phase ϕ_{prec} , is defined as zero when superhump maximum and mid-eclipse coincide. The angle θ_{disc} (see Figure 4) is then $2\pi\phi_{prec}$.

4 RESULTS

The average disc radius R_{disc} in units of orbital separation a is $\langle R_{disc}/a \rangle = 0.32$ with a spread of 0.08. The disc shape is shown in Figure 5 and is clearly not centred on the white dwarf. The shape is similar to that found in OY Car by Hessman et al. (1992).

A good fit to the disc shape was achieved using an ellipse with one focus at the white dwarf, semi-major axis a_{disc} and eccentricity e , described by

$$R_{disc} = \frac{a_{disc}(1 - e^2)}{1 - e \cos(\alpha_{disc} - \alpha_0)}.$$

α_0 is the angle in the precessing disc frame corresponding to maximum disc radius. The resulting fit has $a_{disc} = 0.34a \pm 0.06a$, $e = 0.31 \pm 0.17$ and $\alpha_0 = 117 \pm 33^\circ$ and is shown in Figure 6. The errors in our timing determinations and hence deduced geometry (particularly when using the stream trajectory method) are rather pessimistic; our determinations of a_{disc} , e and α_0 are robust to adopting instead more optimistic error estimates.

The disc is within the tidal cut-off radius $r \sim 0.9R_L = 0.50a$. The largest radius part reaches the location of the 3:1 resonance at $r \sim 0.46a$ (Osaki 1996), providing a possible

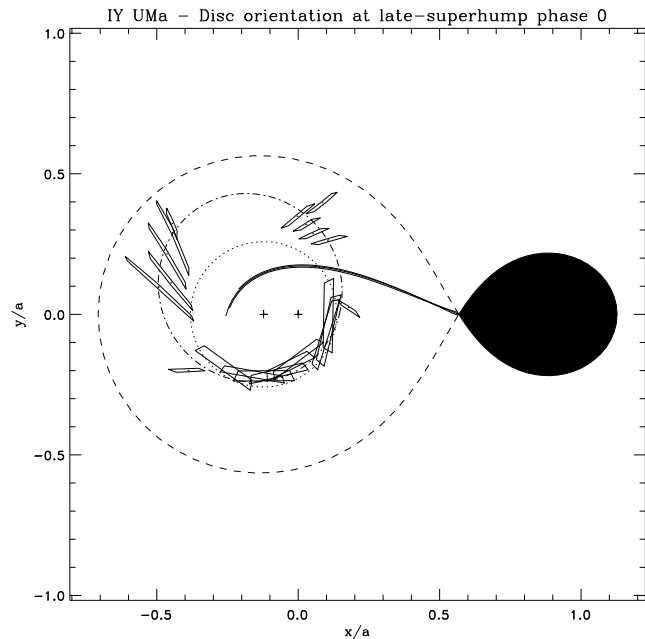


Figure 5. The disc shape traced out from the hot spot ingress and egress times. The disc orientation shown is that which would occur at superhump maximum. Thin regions with large radial extent were determined using the stream trajectory method (Section 3.2). The other regions, which are azimuthally extended (due to the azimuthal extent of the hot spot region and the relative motion of hot spot and disc frame during hot spot eclipse) were determined using the ‘‘shadow’’ method (Section 3.1). The dot-dashed outline is the fitted disc shape and the dotted circle has radius r_{circ} (the circularization radius for mass ratio $q = 0.14$) and is plotted to make the non-axisymmetry of the disc easier to see.

explanation for the maintenance of disc eccentricity at this stage after the superoutburst. The smallest radius coincides with the circularization radius.

5 DISCUSSION

The disc shape we find is similar to that found for OY Car by Hessman et al. (1992), except that we find the minimum radius at disc azimuth $\alpha_{disc} = -63^\circ$ while in OY Car it is around $\alpha_{disc} = 0$. This means the smallest radius of the disc is lined up with the donor star at superhump phase -0.18 in IY UMa while this occurs close to superhump phase 0 in OY Car. This has implications for the viability of the hot spot as the source of the superhump light during the late superhump era. Superhumps caused by the variation in hot spot brightness as the stream impacts the disc at varying depth in the white dwarf potential well were first suggested by Vogt (1981). This theory has generally been rejected as an explanation for the common superhumps occurring during the decline from superoutburst maximum in SU UMa stars, but the possible link between this model and *late* superhumps (which appear during very late decline of the superoutburst) has been suggested several times, e.g. by Whitehurst (1988) and by Rolfe, Haswell & Patterson (2000) (hereafter RHP) after a study of persistent superhumps in the novalike V348 Pup. See RHP for more discussion.

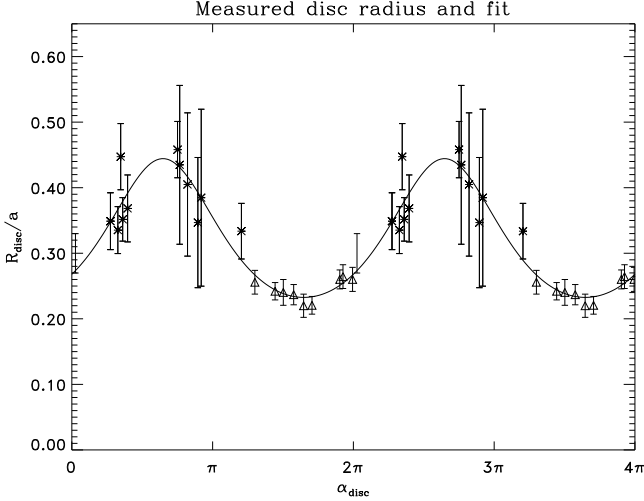


Figure 6. The disc radius as a function of α_{disc} (see definition in Figure 4). Points marked with triangles were determined using the “shadow” method (Section 3.1), while points marked with stars were determined using the stream trajectory method (Section 3.2).

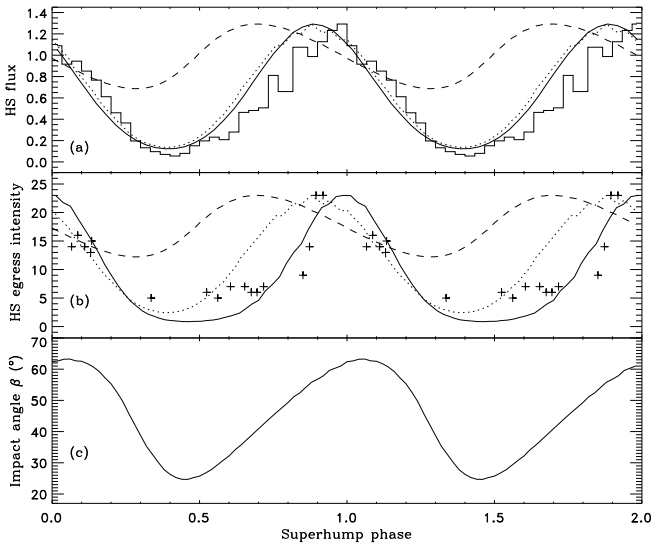


Figure 7. (a) The histogram shows the peak bright spot modulation, obtained by subtracting the normalized average orbital curve from the normalized data and then extracting the data for the orbital phase range 0.85–0.95 and folding on superhump phase. (b) shows the measured hot spot eclipse egress intensity $\Delta I_{h,se}$ (crosses). The dashed curve in (a) and (b) is the kinetic energy of the stream at the hot spot, while the dotted curve is the kinetic energy of relative motion of the stream and disc at the hot spot. The solid curves are the predicted hot spot peak and egress intensities combining our simple 3D model for the hot spot structure with the relative KE model for hot spot brightness. See Section 5. The latter three curves were predicted from the fitted disc shape and scaled in flux to have the same maximum as the measured data. (c) shows the angle β between the stream and disc velocities at the impact point.

In Figure 7a we show a measure of the orbital hump peak modulation while in Figure 7b we show the hot spot flux uncovered on egress of the hot spot eclipse ($\Delta I_{h,se}$ from P2000). The variation in hot spot brightness, $F_{hotspot}$, predicted by our fitted disc shape is shown in Figures 7a & b, calculated using three models described below.

(i) The dashed curve in Figure 7a & b is calculated using $F_{hotspot} \propto 1/r$ where r is the radius of the disc at the hot spot. This assumes the energy released at the hot spot varies as its depth in the white dwarf gravitational potential.

(ii) The maximum energy which could be released at impact is the kinetic energy of the relative motion of the stream and disc at the hot spot. If the stream velocity vector at the point of impact is \vec{V}_{stream} and the disc velocity at this point is \vec{V}_{disc} then the kinetic energy per unit mass of the relative velocity is $KE = \frac{1}{2}(\vec{V}_{disc} - \vec{V}_{stream}) \cdot (\vec{V}_{disc} - \vec{V}_{stream})$. We approximate

$$|\vec{V}_{disc}| = \sqrt{GM_{wd} \left(\frac{2}{r} - \frac{1}{a_{disc}} \right)}$$

at the impact point with direction parallel to the disc edge in the white dwarf frame. This is the correct velocity for an elliptical orbit around a point mass. This model is plotted as the dotted curve in Figures 7a & b.

(iii) The solid curves in Figures 7a & b were produced by assuming the total hot spot flux behaves as described in the previous model, and considering a simple model for the 3 dimensional structure of the hot spot, shown in Figure 8. The hot spot has an elliptical cross section in the $r-z$ plane with axis of size r_{spot} in the radial direction and h_{spot} in the vertical direction (see inset in Figure 8). r_{spot} and h_{spot} and the spot brightness decrease downstream from the initial impact as $e^{-\theta^2/\Delta\theta_{spot}^2}$. Upstream of the impact the hot spot surface is rounded off with a hemisphere of uniform brightness equal to that at the initial impact. The angular extent of the hot spot region is set by $\Delta\theta_{spot} = \Delta\theta_0 a_{disc}/r_0$, where r_0 is the disc radius at the impact point. This keeps the arc length of the hot spot region roughly constant as the eccentric disc precesses. The disc thickness is $2H_{disc} = 0.02a$ and any region of the hot spot surface within the disc is considered to be obscured completely. The total flux coming from an area element on the hot spot surface is foreshortened according to its area projected in the direction of the observer. This simple parametrized model for the hot spot structure enables us to model the full hot spot lightcurve, taking into account the visibility of the hot spot at any orbital phase and disc precession phase. The model lightcurve is shown in Figure 9b. We use $\Delta\theta_0 = 36^\circ$ which is the average azimuthal extent of the hot spot regions determined from the eclipse timings as described in Section 3.1. Noting that we see no eclipse of the white dwarf by the hot spot region, we determine the maximum possible value of h_{spot} for $i = 86^\circ.8 \pm 1^\circ.5$ to be $0.013a \pm 0.006a$. Therefore we use $r_{spot}(\theta = 0) = h_{spot}(\theta = 0) = 0.013a$ at the point of impact.

The phasing of the hot spot brightness predicted by model (i) does not agree with either of the two measures of hot spot variation in Figures 7a & b, with the peak in predicted brightness being about 0.25 earlier than the measured peak. The fractional amplitude in the predicted variation is about half that of the measured variation: in Figures 7a & b

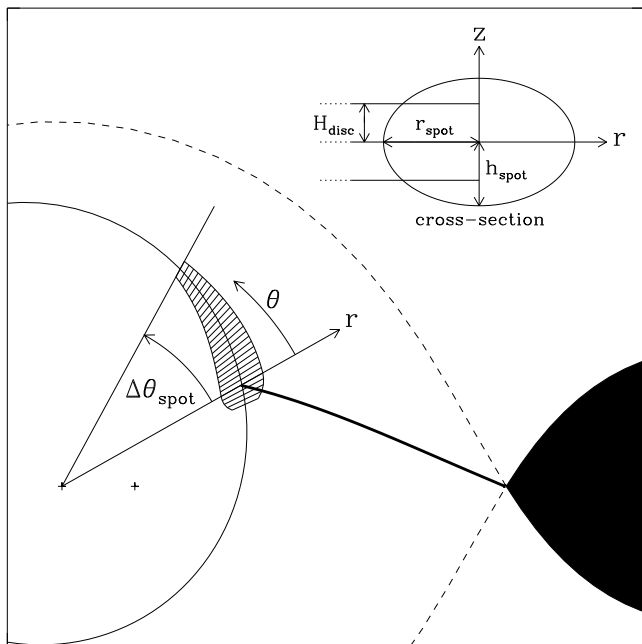


Figure 8. The assumed 3D geometry of the hot spot seen looking down onto the orbital plane in the $-z$ direction. The hot spot is split up into “rings” in the rz -plane which are ellipses centred on the elliptical disc edge with axis in the r direction of r_{spot} and vertical axis h_{spot} . Both r_{spot} , h_{spot} and the hot spot brightness decrease as $e^{-\theta^2/\Delta\theta_{\text{spot}}^2}$ as the stream merges with the disc, and the stream impact is rounded off with a hemisphere for $\theta < 0$.

the predicted curve has simply been scaled to have the same maximum value as the observed hot spot curves.

In Figure 7c we also show the variation of the angle β between the stream and disc velocities at the point of impact (approximately equal to β in Figure 4). The hot spot emission should arise primarily from dissipation of kinetic energy as the infalling stream impacts the disc edge and merges with the Keplerian motion of the disc. The available kinetic energy increases as the angle β between the velocity vectors of the stream and disc flows increases. Figure 7c clearly shows β to be greatest around the observed maximum of the hot spot intensity, which coincides with superhump maximum. This effect is taken into account in model (ii) where the maximum kinetic energy available at the impact point is calculated and depends on the directions and magnitudes of the stream and disc velocities. The shape, phasing and fractional amplitude of the curve for model (ii) shows much better agreement with the hot spot brightness measured in Figure 7a. The predicted curve also agrees well in phase and fractional amplitude with the measure of hot spot flux in Figure 7b, although the hot spot flux between superhump phase ~ 0.6 and 0.9 is much lower than predicted.

Our final model, (iii), which combines the relative kinetic energy model with a treatment of the hot spot visibility, does not differ from the previous model in its prediction for the peak flux of the orbital hump (Figure 7a). This is to be expected since at the peak of the orbital hump we should be seeing the whole length of the bright spot clearly, so the visibility at this orbital phase should not be very sensitive to small changes in orientation through the disc precession cycle. The hot spot flux measured using the hot spot eclipse

egress is different from the predicted variation in intrinsic hot spot flux. This is because at the orbital phase of hot spot egress, we are seeing the impact region roughly end-on, and at this orientation the fraction of the hot spot flux reaching the observer is sensitive to the exact orientation of the hot spot. The result is that the predicted variation (solid curve in Figure 7b) rises to maximum later than the intrinsic variation, but decreases at about the same time as the intrinsic variation. This produces a more flat-bottomed curve which agrees better in shape with the observed egress flux than models (i) and (ii). The flux around egress flux minimum is too low in our models, but this is not surprising; our model for the structure of the impact region is a very simple one. It is also possible that the hot spot emission is strongly anisotropic due to the complicated structure of shocks and contact discontinuities we expect to be present at the impact.

Figure 9a shows the evolution of the IY UMa lightcurve throughout the late superhump era. The important features to note are how strongly the amplitude of the orbital hump varies, and how the late superhump is very weak, in many cases undetectable, when it does not occur near the orbital hump. Strong variation in hump amplitude was also seen towards the end of a more recent superoutburst of IY UMa (Uemura 2000). The combined lightcurve of the late superhump and the orbital hump is not simply a sum of the two, it is some non-linear combination, with the combined hump being extremely strong when orbital hump and late superhump coincide, while both orbital hump and late superhump are weak when they are not coincident. This is exactly what we expect if the stream-disc impact is the source of the late superhump. The hot spot is modulated at the late superhump period, as the impact geometry of the stream and disc varies. Consequently, the orbital hump, which is just the emission from the hot spot coming into view, is modulated on the disc precession period, being strongest at late superhump maximum. The late superhump is very weak away from the orbital hump since away from the orbital hump the bright spot is on the far side of the disc and hence has a low visibility. Our model hot spot lightcurves produced using model (iii) are shown in Figure 9b. Ignoring the stochastic flickering in the observations (which is strongest in the second panel, HJD 72.7), and the deep white dwarf eclipse in the observations not included in the model, our simple model does a convincing job of reproducing the observed bright spot behaviour, although the peak of the orbital hump when it occurs close to late superhump maximum is sharper in the observations than in our model.

The intrinsic bright spot flux in the lightcurve in the third panel (HJD 73.7) appears to be lower than the observed flux, which makes it difficult to see how the shape of this curve agrees with observations. Figure 9c shows the model and observations for this curve, with the model scaled by a factor of 5. The good agreement between the shape of the model and the observations is clear, particularly the double humped nature of each orbit curve and the flattish top to the orbital hump before some of the eclipses. More detailed modeling is necessary to explain the low intrinsic brightness of the hot spot in this region of the disc precession cycle. The relative height of the hot spot peak above the disc needed a bit of fine-tuning to achieve this match between the model

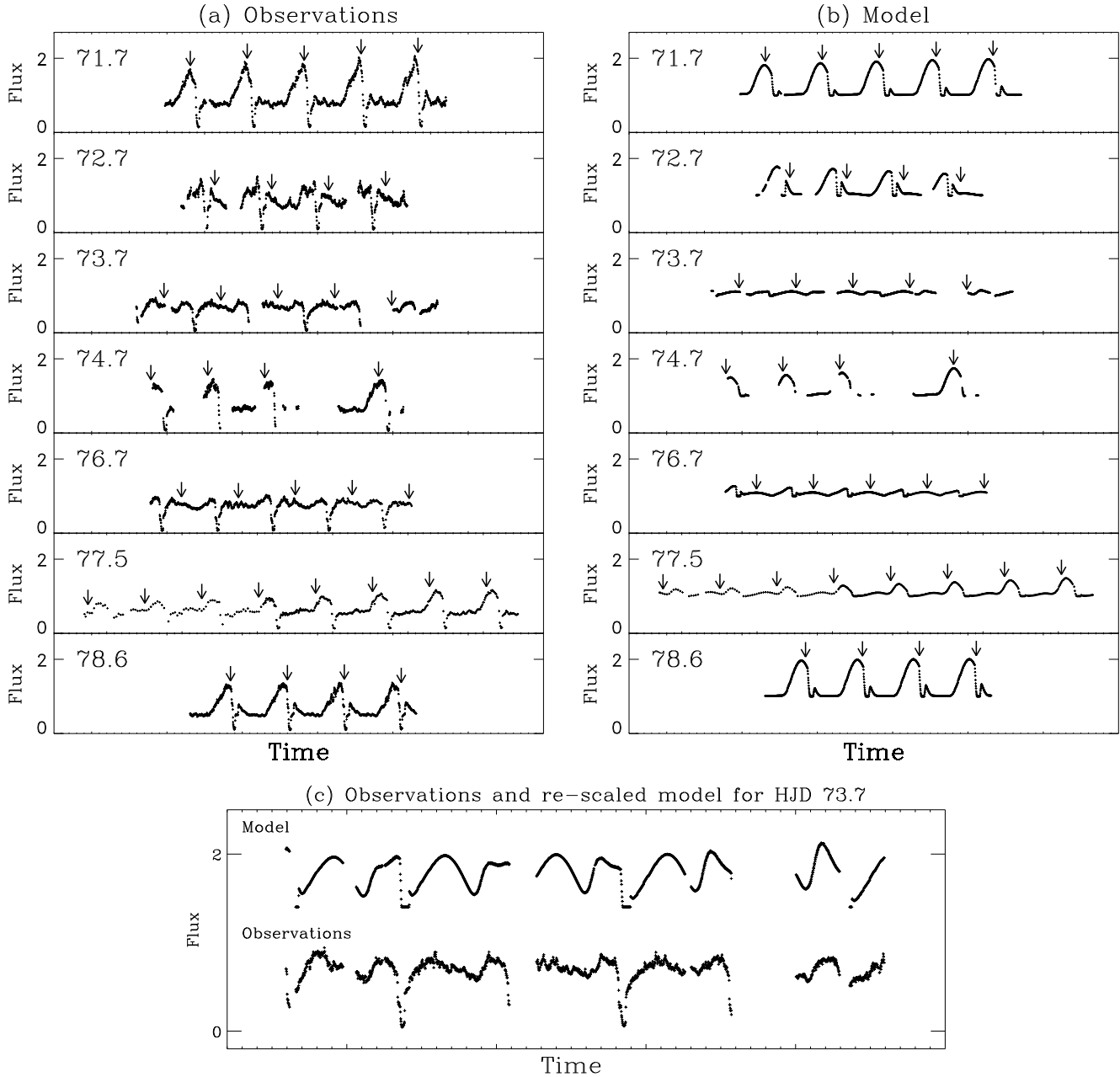


Figure 9. (a) shows all 7 lightcurves from the late superhump dataset analysed in this paper. The date of the start of each lightcurve is shown in the top left of each plot as HJD-2451500. Arrows indicate times of late superhump maximum according to the ephemeris in P2000. Note the significant variation in the amplitude of the orbital hump over the 7 days. (b) Shows our model of the bright spot lightcurve for the same time series as (a). The model assumes the intrinsic hot spot brightness to vary as the kinetic energy of relative motion of stream and disc at impact, while a simple model for the 3D structure of the hot spot enables us to predict its visibility as a function of orbital phase and precession phase. See Section 5. (c) shows the model data from from the 3rd panel of (b) scaled in flux by a factor of 5 and shifted up by 1.4 flux units, along with the corresponding observed data. This shows how the shape of the model lightcurve is morphologically close to that of the observations, although the intrinsic hot spot brightness predicted by our model is too low at the disc precession phase. Note that our model does not include the deep white dwarf eclipse seen in the observations.

and observed lightcurves, and $r_{spot}(\theta = 0)$ had to be less than about twice $h_{spot}(\theta = 0)$.

It is difficult to avoid the conclusion that the late-superhump light in IY UMa is predominantly coming from the hot spot, whose brightness is modulated at the superhump period as a result of the varying impact geometry of the stream and the disc. The disc shape and orientation

found in OY Car (Hessman et al. 1992) suggests that the late superhumps in that system may also originate from the hot spot. An analysis of the OY Car observations like that in our Figure 7 would be valuable. Murray (1996) performed SPH simulations which support the hot spot as the source of late superhump light, but radiative processes were not modelled. More detailed hydrodynamic simulations concen-

trating on the stream-disc impact region have been carried out (e.g. Armitage & Livio 1998), but there has been no study of the hot spot in such detail for non-circular discs. Such work would be valuable in the light of these observations.

We have assumed the shape of the disc to be fixed and constant in the precessing disc frame, while our observations of V348 Pup (RHP) and SPH simulations (Haswell, King, Murray & Charles 2000) suggest the disc shape and size changes during the superhump cycle. The disc shape we find represents the disc radius seen by the accretion stream as a function of superhump phase, and any effect of changing shape should have little effect on the angle β at which the stream impacts the disc since the shape is traced out between radius measurements which are closely spaced in superhump phase.

The transition from the common superhumps which appear during the decline from maximum of the superoutburst to the late superhumps during the very late decline of the superoutburst is easy to explain using a minor modification to the tidal-thermal-instability model of Osaki (1989) proposed by Hellier (2000). Hellier suggests that the tidal and thermal instabilities are uncoupled: the disc can drop out of the thermal high state at the end of the superoutburst while remaining tidally eccentric. At this point, the disc viscosity dramatically reduces and so the viscous dissipation due to tidal stressing which causes normal superhumps will be similarly reduced, allowing the late superhumps which were drowned out during the superoutburst to be seen.

6 SUMMARY

The timing of hot spot eclipses during the late superhump era reveals the disc shape, which proves to be non-axisymmetric.

The inferred shape and orientation of the disc and a simple treatment of the kinetic energy available at the stream-disc impact enable us to calculate the hot spot brightness throughout the superhump cycle. The resulting variation in predicted hot spot brightness matches the observed variation well, and is in very close agreement with the superhump modulation. Combining these results with a simple model for the 3D structure of the hot spot enables our model to reproduce the observed lightcurves during the late superhump era.

We conclude that the stream-disc impact region is the source of late superhump light in IY UMa.

7 ACKNOWLEDGEMENTS

The authors are very grateful to Jonathan Kemp, Tonny Vanmunster and Bob Fried who contributed the data analysed here. We acknowledge the data analysis facilities at the Open University provided by the OU research committee and the OU computer support provided by Chris Wigglesworth. We thank Andrew King and Ulrich Kolb for helpful advice and discussion, and Rick Hessman whose suggestion prompted this work. The comments from the anonymous referee are also appreciated. DJR is supported by a

PPARC studentship. CAH gratefully acknowledges support from the Leverhulme Trust F/00-180/A.

REFERENCES

- Armitage P.J., Livio M., 1998, *ApJ*, 493, 898
 Baraffe I., Chabrier G., Allard F., Hauschildt P.H., 1998, *A&A*, 337, 403B
 Haswell C.A., King A.R., Murray J.R., Charles P.A., 2000, *MNRAS*, in press, astro-ph/0008367
 Hellier C., 2000, presented at 'Evolution of binary and multiple star systems, a conference in honour of Peter Eggleton's 60th birthday', Bormio, Italy
 Hessman F.V., Mantel K.-H., Barwig H., Schoembs R., 1992, *A&A*, 263, 147
 Murray J.R., 1996, *MNRAS*, 279, 402
 Osaki Y., 1989, *PASJ*, 41, 1005
 Osaki Y., 1996, *PASJ*, 108, 39
 Paczyński B., 1977, *ApJ*, 216, 822
 Patterson J., Kemp J., Jensen L., Vanmunster T., Skillman D.R., Martin B., Fried R., Thorstensen J.R., 2000, *PASP*, accepted (P2000)
 Rolfe D.J., Haswell C.A., Patterson J., 2000, *MNRAS*, 317, 759 (RHP)
 Uemura M., 2000, *VSNET Weekly Campaign Summary* (531), Oct. 17 2000
 Uemura M., Kato T., Matsumoto K., Takamizawa K., Schmeer P., Jensen L.T., Vanmunster T., Novák R., Martin B., Pietz J., Buczynski D., Kinnunen T., Moilanen M., Oksanen A., Cook L.M., Watanabe T., Maehara H., Itoh H., 2000, *PASJ*, in press
 Vogt N., 1981, *ApJ*, 252, 653
 Wood J.H., Horne K., Berriman G., Wade R., O'Donoghue D., Warner B., 1986, *MNRAS*, 219, 629
 Whitehurst R., 1988, *MNRAS*, 232, 35